Statyba

ISSN: 1392-1525 (Print) (Online) Journal homepage: https://www.tandfonline.com/loi/tcem19

EXPERIMENTAL AND NUMERICAL ANALYSIS OF THIN-WALLED BARS IN COMPRESSION AND BENDING

Dr Habil A. Biegus

To cite this article: Dr Habil A. Biegus (2000) EXPERIMENTAL AND NUMERICAL ANALYSIS OF THIN-WALLED BARS IN COMPRESSION AND BENDING, Statyba, 6:4, 247-254, DOI: 10.1080/13921525.2000.10531596

To link to this article: https://doi.org/10.1080/13921525.2000.10531596

Published online: 26 Jul 2012.

ISSN 1392-1525. STATYBA - CIVIL ENGINEERING - 2000, VI tomas, Nr. 4

EXPERIMENTAL AND NUMERICAL ANALYSIS OF THIN-WALLED BARS IN COMPRESSION AND BENDING

A. Biegus

Wroclaw University of Technology

1. Introduction

Corrugated metal sheeting normally used for roofing decking or side-cladding are subjected to cross-bending loads and the ones acting in its plane like compression. Such combination of loading occurs, for instance, in the compound, integral truss girder in which the upper flange is designed as a sheeting profile – 1, when me rest of me unit is made of bars – 2, 3, 4 (Fig 1).

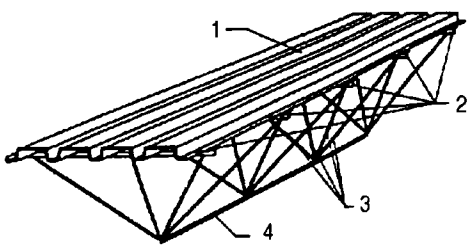

Fig 1. Scheme of the plate–girders

Theoretical investigations of Easley [1], Hlavacek [2] and experiments executed by Bryan [3], [4] Davies [5] and Easley [1], [6] have considered the pure in plane shearing without the participation of transversal and compression forces. The main attention was paid to the flexibility of sheeting profile under shearing. For the sheeting profile sufficiently fixed to the rest of the structure the exhaustion of the load capacity can be caused by the interaction of bending and compression (for slender elements) or by combined bending and shear.

The literature review shows the necessity of a deeper analysis of the load-bearing capacity enriched by cases mentioned above. In this paper a method for estimating the load-bearing capacity based on the interaction curve M–N has been proposed for the thin-walled monosymmetrical bars under compression and bending. The interaction curves have been based on the analysis of the stress-displacement distribution and the experimental values of the load bearing capacities recorded for unaxially compressed corrugated sheets, which was additionally supported by the mathematical model set up for bars loaded as mentioned. This paper presents the results of tests carried out on 20 models full-scale of corrugated sheet compression N in the plane of diaphragm. Numerical model of the thin-walled bar under bending and compression given as a differential equation of the fourth order with non-linear coefficients combines the second order bending theory with the Winter's effective width conception [7].

The most frequently used symbols:

a, b, c, h, r – cross-sectional dimensions (Fig 2),

a_e, b_e, h_e – effective widths of compression element,

e – eccentricity of compressing force N,

t – thickness of thin-walled bar,

l – length of a bar,

q – transversal load,

y – deflection,

y_0 – eccentricity of compressing force caused by the new position of the profile neutral axis,

E – modulus of elasticity,

J, J_e – moment of inertia of gross cross-section, effective cross-section,

A, A_n, A_e – area of gross cross-section, net cross-section, effective cross-section,

M, N – axial force, bending moment,

M_{ef}, M_{el}, M_{pl} – effective, elastic, plastic bending capacity,

$N_{pl}, N_{cr,e}, N_u$ – plastic, critical capacity and load-bearing capacity,

W, W_{pl}, W_e – modulus of gross cross-section, modulus of plastic cross-section in flexure, modulus of effective cross-section in flexure,

σ, σ_{cr} – normal and critical compressive stresses of thin-walled profile,

f_y – yield stress, design value,

λ, λ_s – slenderness parameter: of a bar in compression, of flanges and webs in compression.

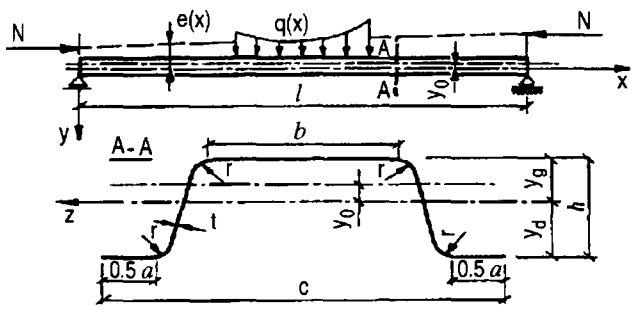

Fig 2. Scheme of the corrugated sheet in compression

2. Tests on eccentrically compressed corrugated sheet

The tests were carried out on full-scale models made from T55x188 corrugated sheets of 750 mm width, 2000 mm length and 0.75 mm and 1.00 mm thickness. The tests were run for two schemes of compressive loads: two forces N_w applied to the upper flange or two forces N_n applied to the lower one. 5 models for each thickness for two shims of loading (Figs 3 and 4) were tested.

The models of corrugated sheet were put on a test stand and subjected to a monotonically growing load. The load was transferred in a way that insured articulation and protected against local failure. The vertical displacement was measured at 10 points and the strain at 22 points in the middle of the models' span length. The deflection and the strain were measured at every 2 kN.

The mean yield points of the sheets were for:

- t = 0.75 mm – $f_{y,1}$ = 337,8 MPa,
- t = 1.00mm – $f_{y,2}$ = 342,9 MPa.

Local buckling of the wider flanges was observed already at the initial stage of loading models eccentrically compressed by a force applied to the wider flange of the corrugated sheet. The amplitudes of the waves of two adjacent fields had opposite signs and the waves disappeared after unloading. No waves in the webs were noticed.

No local buckling of wider flanges, narrower flanges or webs was observed during the eccentric com-

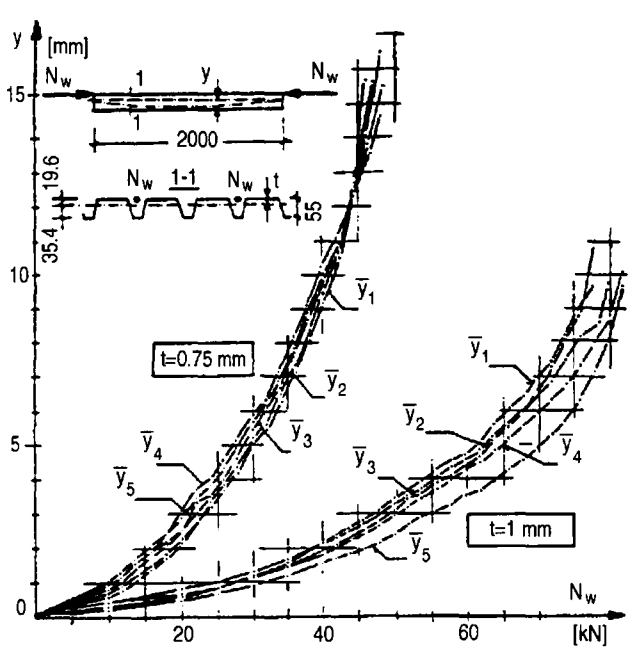

Fig 3. Deflections of the sheets $\bar{y}_i$ eccentrically load N_w

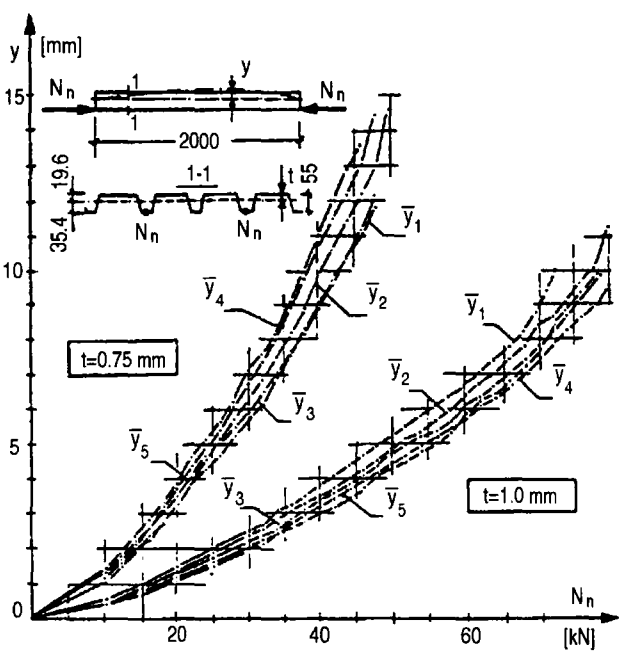

Fig 4. Deflections of the sheets $\bar{y}_i$ eccentrically load N_n

pression of the models by a force applied to the narrower flange. Only in one model of this series, ie the one with the 0.75 mm thick sheet, local buckling of the narrower flange was observed under the toad about 1 kN below the limit load.

The deflections of the folds of two series of models had the same sign and grew as the load increased. The coefficients of variability (interclass ones) of the folds' deflections decreased as loads increased. Non-linear increment in the tested models displacement was observed during the whole process of loading.

The failure phenomenon of the eccentrically compressed models consisted in a sudden, random, local plastic hinge of one fold: a wider one, when the wider flanges were compressed, and a narrower one, when the narrower flanges were compressed. The hinge was located randomly along the fold's length. Both the extreme fold and the middle fold failed. The phenomenon was accompanied by a sound effect. The collapse of the wider flange was coupled with the failure of the adjacent webs. The plastic hinge was permanent. Other folds still did not fail. The failure of one fold was accompanied by a sudden drop in the compressive force (the compressive load had a nonconservative character). An attempt to increase the load on the models resulted in the depletion of the load-bearing capacity of the consecutive folds, an increase of the displacement and a drop in the loading force. The mechanism of the models failure consisted in the formation of four plastic hinges of the sheet's folds.

Figs 3 and 4 show diagrams of the deflections of models $\bar{y}_i$, of 0.75 and 1.00 mm thick sheets as a function of eccentric loads N_w applied to the wider flange and loads N_n applied to the narrower one. Deflections y – the interclass ones were calculated as the mean deflection of the folds of a given model (the mean from 8 measuring points).

The interclass diagrams (the mean from 5 models) of deflections $\bar{y}_w, \bar{y}_n$ of the sheets are shown in Fig 5.

The extensometer studies of the eccentrically compressed corrugated plates have shown that the structures' load-bearing capacity becomes depleted as a result of the stiffener plasticisation of the compressed thin-walled sections. The stiffener of a section constituted „supporting" members for the compressed, waved flange. The depletion of the stiffener load-bearing capacity leads to the fold plastic hinge.

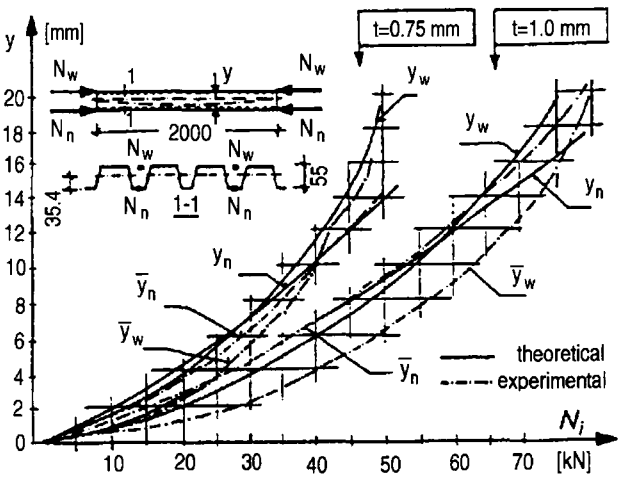

Fig 5. Experimental and numerical deflections of sheets

The collapsed fold drops and the redistribution of forces results in the overloading other folds (the ones that have not failed yet) leading to a similar mechanism of failure in them. The load-displacement curve $N(y)$ of the eccentrically compressed corrugated plates are non-linear functions. These curves are characterised by a lack of the plastic stage in the structure's work (in case of compressed thin-walled bars). The load-displacement curves of the eccentrically compressed corrugated plates can be described by a non-linear-elastic-brittle model having the following parameters: rigidity $EJ(N)$ and limit load-bearing capacity N_u.

3. Mathematical model of thin-walled bars under bending and compression

The thin-walled bar subjected to compression axially N is shown in Fig 2 ($e = 0$, $q(x) = 0$). The equilibrium state in the elastic range for me thin-walled bar for his gross section ($\sigma < \sigma_{cr}$) can be expressed as:

$$EJy^{IV} + Ny^{II} = 0. \qquad (1)$$

The stress distribution becomes non-linear [7] after local buckling of flanges or webs $\sigma > \sigma_{cr}$. According the Winter's theory of the effective width, the dimensions are changed as follows: $a \to a_e(N)$, $b \to b_e(N)$, $h \to h_e(N)$ as a function of the load N. Thus, the flexural rigidity becomes:

$$J(a,b,c,h,t,r)_{\sigma<\sigma_{cr}} > J_e(N) = J_e[a_e(N),b_e(N),c,h_e(N),t,r]_{\sigma>\sigma_{cr}} \quad (2)$$

and the bar loaded axially for $\sigma<\sigma_{cr}$ ($y_0=0$) is compressed eccentrically for $\sigma>\sigma_{cr}$. The eccentricity of a load y_0 depends on the load as well:

$$y_0 = y_0[a_e(N),b_e(N),c,h_e(N),t,r]_{\sigma>\sigma_{cr}}. \quad (3)$$

Unaxial compression causes nonuniform stress distribution so, that the equation (1) written for $\sigma<\sigma_{cr}$ changes its shape to the differential equation with nonlinearly changing coefficients for combined bending and compression ($\sigma>\sigma_{cr}$).

$$\left[EJ(N)y^{II}\right]^{II} + \left\{N\left[y^{I} + y_0^{I}\right]\right\}^{I} = 0. \quad (4)$$

Of course, the solution of the equation (4) does not lead to me value of the mathematical critical load although the initial load acted axially. Instead of this displacements, bending moments and shear forces can be determined as a function of the load *N*, according to the second order theory. For a bisymmetrical cross-section the problem is reduced to the changing of the flexural rigidity only, $EJ_e = EJ(N)$ and we are still facing the pure overall buckling. In case, when the monosymmetrical bar (Fig 2), initial rigidity $EJ(\sigma<\sigma_{cr})$ is loaded unaxially by the load N, and additionally by the transversal load $q(x)$ the equilibrium equation for $\sigma>\sigma_{cr}$ is:

$$\left[EJ(N,q,x)y^{II}\right]^{II} + \left\{N\left[y^{I} + y_0^{I}(N,q,x),e^{I}(x)\right]\right\}^{I} = 0. \quad (5)$$

As before, we are getting fourth order differential equation with non-linearly changing coefficients, ie rigidity $EJ(N, q, x)$ and eccentricity $y_0(N, q, x)$. The load-displacement relationship for mis bar in $N - y$ co-ordina-tes is non-linear due to the flexural rigidity reduction and the growing eccentricity $y_0(N, q, x)$. Depending on the geometry of the thin-walled cross-section, the length l, and the eccentricity, we can have three forms of the load capacity exhaustion: the plastic hinge of a fold (Fig 6 c), the plasticisation of the tensiled portion of me cross-section (Fig 6 b) or the classic lost of the stability for $e = 0$ and $\sigma<\sigma_{cr}$ for monosymmetrical bars or for $e = 0$, when the bar has a bisymmetrical cross-section (Fig 6 a) [8].

In the thin-walled elements under bending, the relationship loading-deflection remains linear for $\sigma<\sigma_{cr}$. After local buckling of the compressed flanges the redistribution of stresses changes the position of the neutral axis, the relationship loading-deflection becomes non-linear. The position of the monosymmetrical beam neutral axis does not cause any additional stresses in the contrary of combined bending and compression.

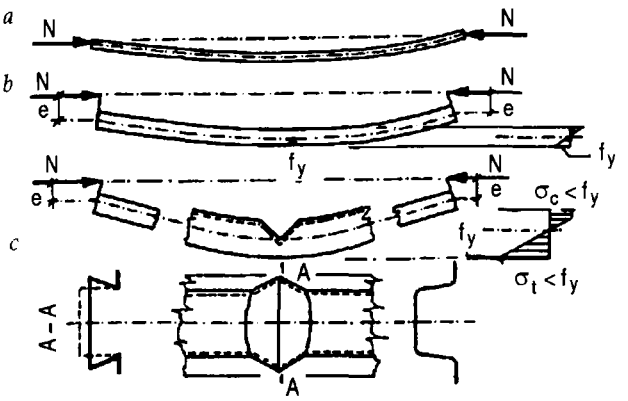

Fig 6. Model of the corrugated sheet collapse

The bars with variable rigidity have been considered by many authors, among them by A. Kacner [9] and S. P. Timoshenko [10]. In paper [11] the equation (5) for bars with changing rigidity is solved by means of trigonometric series applying the finite Fourier transformation.

It is proposed to calculate the load-bearing capacity and the relationship load-displacement using the incremental method step by step since characteristics $A(N, q, x)$, $W(N, q, x)$, $J(N, q, x)$, and eccentricity $y_0(N, q, x)$, are dependent on compressive load N. For this purpose a special program NSEC has been developed [11], which allows to analyse the behaviour of the axially and unaxially compressed thin-walled bars having a monosymmetrical hat cross-section (Fig 2). The program NSEC gives in me output the values: $a_e, b_e, h_e, J_e, A_e, y_0, y$, extreme fibre stresses starting from initial loading N_0 incrementally (ΔN) up to the load-bearing capacity or up to the critical load.

4. Interaction functions *M–N* for thin-walled bars under compression and bending

The proposed mathematical model, its solution [11] and the developed program [8] give basis for load-bearing estimation of the bars under combined bending and compression. The shape of the interac-

tion curves M–N has been analysed for corrugated sheets T55xl88 with thickness 0.5; 0.75; 1.0 and 1.25 mm.

For bars under tension, the load-bearing capacity is:

$$N_{pl} = A_n f_y . \tag{6}$$

For thin-walled bar in bending there are two cases to be considered. First, when normal stress σ_i is less than $\sigma_{cr,i}$ for all walls of the cross-section no reduction is reasonable and the load-bearing capacity is calculated from the formula:

$$M_{pl} = W_{pl} f_y . \tag{7}$$

For corrugated sheets this case is rather theoretical. More likely is the other case when local buckling occurs in compressed flanges $\sigma_i > \sigma_{cr,i}$, hen the load-bearing capacity of the bar under bending is:

$$M_e = W_e f_y . \tag{8}$$

The load-bearing capacity in the elastic range for the thin-walled bar has been taken theoretically as:

$$N_{cr,e} = \frac{\pi^2 E J_e}{(\mu l)^2} . \tag{9}$$

To achieve such a state ($N_u = N_{cr}$) is technically difficult owing to random imperfections. Theoretically it is possible by loading at the eccentricity equal to the displacement of the neutral axis ($e = y_0$) in the limit state. Actually a bar is loaded at eccentricity e caused by the displacement of the neutral axis due to changing effective widths, therefore the load capacity can be calculated by formula:

$$N_u = \frac{W_e A_e f_y}{W_e + A_e (e + y_0)\eta} , \tag{10}$$

in which

$$\eta = \beta (1 - N / N_{cr,e})^{-1} , \tag{11}$$

where y_0 is displacement of the neutral axis in the limit state stress $\sigma_i > \sigma_{cr,i}$, β is corrective coefficient with respect to the diagram of bending moments along the bar.

Rigidity characteristics for tested thin-walled bars

t mm	Way of loading	b_e mm	h_e mm	a_e mm	A_e cm²	y_g cm	J_e cm⁴	W_{ew} cm³	W_{en} cm³	W_{pl} cm³	$\frac{W_{e(w,n)}}{W_{pl}}$	$\frac{N_{cr}}{N_{pl}}$
1	2	3	4	5	6	7	8	9	10	11	12	13
0,50	B_{nom}	114,0	43,00	32,00	1,364	1,930	6,759	3,502	1,893	2,567	0,737	0,408
	B_w	23,36	43,00	32,00	0,906	2,895	4,162	1,437	1,597		0,560	
	B_o	22,36	20,63	19,67	0,620	2,691	3,725	1,384	1,326			
	B_n	114,0	43,00	19,67	1,302	1,763	5,964	3,383	1,596		0,622	
0,75	B_{nom}	114,0	43,00	32,00	2,050	1,936	10,07	5,204	2,827	3,872	0,730	0,475
	B_w	32,75	43,00	32,00	1,441	2,739	6,832	2,494	2,473			
	B_o	32,75	28,86	26,72	1,189	2,647	6,514	2,461	2,283			
	B_n	114,0	43,00	26,72	2,010	1,867	9,583	5,133	2,638		0,681	
	B'_w	32,93	43,00	32,00	1,422	2,736	6,840	2,500	2,475		0,650	
1,00	B_{nom}	114,0	43,00	32,00	2,740	1,942	13,37	6,886	3,758	5,202	0,722	0,534
	B_w	42,62	43,00	32,00	2,027	2,608	9,794	3,755	3,386			
	B_o	42,62	35,71	32,00	1,881	2,598	9,791	3,769	3,374			
	B_n	114,0	43,00	32,00	2,740	1,942	13,37	6,886	3,758		0,722	
	B'_w	45,08	43,00	32,00	2,051	2,578	10,08	3,910	3,449		0,633	
1,25	B_{nom}	114,0	43,00	32,00	3,432	1,947	16,65	8,551	4,686	6,529	0,717	0,564
	B_w	53,97	43,00	32,00	2,656	2,497	12,95	5,187	4,313			
	B_o	51,97	41,17	32,00	2,610	2,493	12,95	5,194	4,307			
	B_n	114,0	43,00	32,00	3,432	1,947	16,65	8,551	4,686		0,717	
	B'_w	57,42	43,00	32,00	2,724	2,436	13,48	5,537	4,402		0,674	

The interaction curves M–N shown in Fig 7 have been used for determining the load-bearing capacity of the bar T55x188, of length $l = 2000$ mm, of slenderness $\lambda = 90$, where the stresses have been calculated with respect to the bending moment calculated according to the first order theory. The diagrams M–N (Fig 7) are plotted on the basis of calculation executed according to the program NSEC [8], for hat cross-sections with thickness 0.5; 0.75; 1.0; 1.25 mm and $f_y = 340$ MPa.

Rigidity characteristics of the considered thin-walled bars (corrugated sheet T55x188, thickness 0.5; 0.75; 1.0; 1.25 mm) are presented in Table: in the lines B_{nom} the nominal characteristics (when $\sigma_i < \sigma_{cr,i}$), in the lines B_w, characteristics for a cross-section with compressive stresses acting in the wider flange, in the lines B_0, characteristics for a cross-section axially compressed ($e = y_0$) and $\sigma = f_y$ in flanges and webs, in the line B_n characteristicss for $\sigma = f_y$ in the narrower flange under compression in lines B'_w characteristics for $\sigma_{wide} < f_y$ (compression) in the wider flange and $\sigma_{narrow} = f_y$ (tension) in the narrower flange.

For a given eccentricity e, the compressive load-bearing capacity has been calculated by the program NSEC, afterwards the bending moment M according to the first order theory and finally the co-ordinates of the interaction curve M/M_{pl}, N/N_{pl}.

When stresses in the compressed flanges are bigger than critical stresses of a local budding the flexural rigidity has to be reduced, the maximal bending moment for an effective cross-section for $N = 0$ can be calculated from the relation (8), so that:

$$M_e < M_{el} < M_{pl} \qquad (12)$$

(M_{el} is elastic bending moment of the gross cross-section).

The elastic modulus of me gross cross-section to plastic section modulus ratio is given in Table, col. 12, line B_n. The elastic modulus of the effective cross-section (reduced width in flanges) to plastic section modulus ratio W_e/W_{pl} is given in Table, col.12 lines B_w and B_n or B'_w. It has to be mentioned that the ratio W_e/W_{pl} is different for the compression of the narrower flange from that in the wider flange and depends on the stress grade and is lesser than W/W_{pl}.

The load-bearing capacity of the cross-section in bending ($N = 0$) or for very small compressive stresses due to N_w depends on the tensile zone capacity (characteristics from line B'_w). This case occurs (Fig 6 b) for the bars with thickness t = 0.75; 1.0 and 1.25 mm.

The maximal ratio M/M_{pl} may not appear on the vertical axis – for $t = 1.25$ mm and $N/N_{pl} = 0.04$ (Fig 7) we are getting a local extremum.

The maximal compressive force for $M = 0$ is:

$$N_{pl,e} = A_e f_y, \qquad (13)$$

and occurs for bars with small slenderness, loaded at an eccentricity $e = y_0$ in limit stress state ($\sigma_i > \sigma_{cr,i}$).

The load $N_{pl,e}$ can be carried out by bars with very small slenderness: bisymmetrical, loaded axially or monosymmetrical, loaded unaxially when $e = y_0$. With the growing slenderness, the compressive load-bearing capacity is getting smaller. The critical load (9) of the bars with λ = 90 and f_y = 340 MPa with effective width to plastic load ratio $N_{cr,e}/N_{pl}$ is presented in Table, col. 13. Also, in this case $N_{pl,e}/N_{pl}$ and $N_{cr,e}/N_{pl}$ is getting smaller when both the stresses and slenderness of webs and flanges are growing.

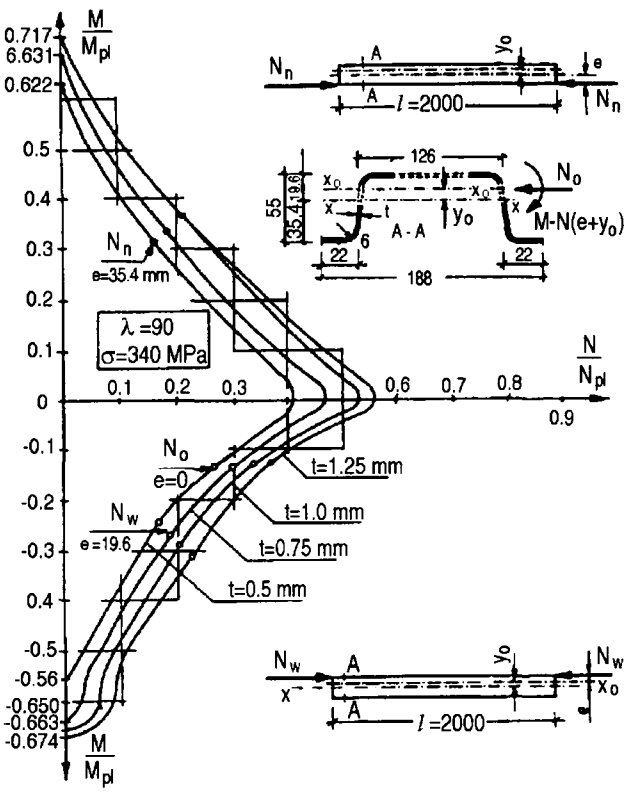

Fig 7. Interaction curves M–N of the bars λ = 90

In the upper part of Fig 7 (t = 1.0 and 1.25 mm), a case is shown when compressive stresses in the narrower flange fulfill the condition $\sigma_i < \sigma_{cr,i}$. Then the interaction curves are not dependent on the slenderness of the compressed flanges up to 0.30 N_{pl}.

The interaction curves of combined bending and compression are shown on the upper and bottom part of Fig 7, for t = 0.5 and t = 0.75 mm when the condition $\sigma_i > \sigma_{cr,i}$ is valid and the reduction of the cross–section area is recommended.

For four thicknesses of considered bars with $\lambda = 90$ we have got four concave curves. The interaction curves M–N for $\sigma_i > \sigma_{cr,i}$ apart from overall slenderness are also the function of slenderness of the flanges λ_s under compression and cross-sectional stresses. Both the cross-sectional area reduction and the effect of displacement y_0 on the cross-sectional stresses cause the concave shape of the curves. The analysed case of combined bending and compression of a thin-walled bar locally buckled is described by the expression:

$$\frac{N N_{pl,e}}{A_e N_{cr,e}} + \eta \frac{M_q + N(e + y_0)}{W_e (1 - N / N_{cr})} \le f_y , \qquad (14)$$

where

M_q is bending moment with respect to transversal loading. Substituting expressions (8), (13) and (14) we get:

$$\frac{M_q + N(e + y_0)}{M_e} \eta \le \left[1 - \frac{N}{N_{cr,e}} \right]^2 . \qquad (15)$$

5. Conclusions and final remarks

The depletion of load-bearing capacity of the eccentrically compressed corrugated sheet consisted in formation of plastic hinges in the compressed flanges of thin-walled sections. The $N(v)$ curves for the compressed corrugated plates are characterised by a high coefficient of deflection variation.

A mathematical model of the thin-walled bars under combined compression and bending is described by equation (5). This is a fourth-order differential equation with non-linearly variable coefficients: flexural rigidity $EJ(N, q, x)$ and variable eccentricity of compressive loads $y_0(N, q, x)$ caused be the change of neutral axis position under growing load. Theoretical analysis supported by experimental investigations shows that monosymmetrical, thin-walled bars are usually unaxially compressed which is described by non-linear load-displacement curves $v(N)$. The maximal compressive load in a monosymmetrical thin-walled bar can be gained by loading applied at the eccentricity equal to the neutral axis displacement in the limit stress state ($\sigma_i > \sigma_{cr,i}$) in relation to the initial position in an unloaded.

Interaction curves M–N of monosymmetrical, thin-walled bars under compression and bending depends on many parameters of slenderness: overall A and local of compressed flanges λ_s, state of stresses σ (effective width depends on σ). The interaction M–N is depicted by concave curves which can have local extremities and are not symmetric with respect to the axis N / N_{pl}.

A comparison (Fig 5) between the experimental values $\bar{y}_w, \bar{y}_n$ and the theoretical y_w, y_n ones (determined by the NSEC program) for the load-bearing capacity of the eccentrically compressed plates N_w, N_n shows that the maximum differences are in the interval from – 7,0% to + 5,5%.

References

1. I. T. Easley, D. E. McFarland. Buckling of Light-Gage Corrugated Metal Diaphragms // J. Struct. Div., ASCE 95, ST 7, July 1969, p. 1497–1516.
2. V. Hlavacek. Shear Instability of Orthotropic Panels // Acta Technica CSAV 1/1968, Praque, p. 134–158.
3. E. R. Bryan, M. Davies. Design of Profiled Steel Sheetingand Decking. Behaviour of Thin-Walle Structures. Elsevier, London, 1984.
4. E. R. Bryan. The Stressed Skin Design of Steel Buildings. Constrado Monograph, London, 1973.
5. J. M. Davies. Light Steel Folded Plate Roofs // The Structural Engineer, 5, 1976, p. 159–174.
6. I. T. Easley. Buckling Formulas for Corrugated Metal Shear Diaphragms // J. Struct. Div., ASCE, ST 7, July 1975, p. 1403–1417.
7. G. Winter. Strength of Thin Steel Compression Flanges // Trans. ASCE, 112, 1974.
8. A. Biegus, J. Gierczak. Load Bearing Capacity of Corrugated Sheet in Eccentric Compression // International Colloquium. European Session. Preliminary Report. Technical University of Budapest, 1995, Vol 2, p. 125–132.
9. Kacner. Bars and Plates of Variable Rigidity. PWN, Warszawa, 1969. 185 p.

10. S. P. Timoshenko, J. M. Gere. Theory of Elastic Stability. Mc Graw-Hill Book Company, New York, 1961.

11. A. Biegus. Load Bearing Capacity of Corrugated Sheet under Compression // Prace Naukowe Instytutu Budownictwa Politechniki Wroclawskiej, Monografie Nr. 38, Wroclaw, 1983. 143 p.

Įteikta 1999 11 18

GNIUŽDOMŲ IR LENKIAMŲ PLONASIENIŲ STRYPŲ EKSPERIMENTINĖ IR SKAITMENINĖ ANALIZĖ

A. Biegus

Santrauka

Plieno strypinių konstrukcijų ir pramonės paviljonų stogų ir sienų strypiniai ryšiai vis dažniau pakeičiami profilinių lakštų pertvarinėmis sienomis. Profiliniai lakštai, atlikdami atitvarinę funkciją ir būdami lenkiamaisiais elemetais, tokiuose konstrukciniuose sprendimuose dirba kaip gniuždomosios pertvaros.

Šiame straipsnyje pateikti rezultatai bandymų, atliktų su 20 natūralių matmenų modelių, padarytų iš T55×188×750 profilinių lakštų, kurių storis buvo 0,75 ir 1,00 mm. Profilinių lakštų elementai buvo gniuždomi jėga N iš profilinių lakštų, padarytų petvarų plokštumoje.

Bandymai leido nustatyti apkrovų įlinkių kreives, irimo mechanizmą ir eksperimentinės sąveikos sandarą iš karto veikiant gniuždymui ir lenkimui.

Straipsnyje pateiktos viensimetrių gniuždomų ir lenkiamų plonasienių strypų sąveikos kreivės. Matematinis modelis derina Winterio (*Winter*) pokritinio laikomumo teoriją ir antrosios eilės lenkimo teoriją.

Aptartas sąveikos kreivių sudarymo metodas. Pasiūlytas būdas, kaip įvertinti monosimetrinių, plonasienių, tuo pat metu ir gniuždomų strypų laikomumą. Rezultatai yra iliustruojami strypų, kurių ilgis 2000 mm ir skerspjūvis T55×188, kai jo storis 0,5, 0,75, 1,0 ir 1,25 mm, pavyzdžiais.

Antoni BIEGUS. Professor, Dr Habil. Wroclaw University of Technology, Wybrzeze Wyspianskiego 27, 50–370 Wroclaw, Poland.

MSc (1971), PhD (1976), DSc (1984) degrees from Dept of Civil Engineering, Wroclaw University of Technology.

Professor of structural steel design and a practising consultant engineer for structural steel projects. Author of more than 90 papers and 9 books in field metal structures. Research interests: space structures, bearing capacity of thin-walled bars, analysis of elastic-plastic structures and reliability.